Available online at www.sciencedirect.com

ScienceDirect

journal homepage: www.elsevier.com/locate/he

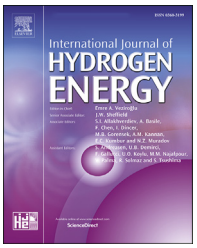

Ti–Fe mixed oxides as photocatalysts in the generation of hydrogen under UV-light irradiation

A. Pérez-Larios [a,c,*], M.I. Torres-Ramos [a], O.A. González-Vargas [d], José L. Rico [b], R. Zanella [c]

[a] Laboratorio de Investigación en Materiales, Agua y Energía, Engineering Department, Campus Los Altos, University of Guadalajara, Av. Rafael Casillas Aceves 1200, Tepatitlan de Morelos, Jalisco, 47600, Mexico
[b] Department of Chemical Engineering, Laboratorio de Catálisis, Universidad Michoacana de San Nicolás de Hidalgo, Morelia, 58060, Mexico
[c] Instituto de Ciencias Aplicadas y Tecnologia, Universidad Nacional Autónoma de México, Circuito Exterior S/N, 04510, Mexico City, Mexico
[d] Departamento de Ingeniería en Control y Automatización, Escuela Superior de Ingeniería Mecánica y Eléctrica-Zacatenco, Instituto Politécnico Nacional, UPALM, Av. Politécnico S/N, Col. Zacatenco, Alcaldía Gustavo A. Madero, Ciudad de México, 07738, Mexico

HIGHLIGHTS

- Ti–Fe as mixed oxide is proposed improve hydrogen generation.
- Ti–Fe nanocomposite exhibiting agglomeration and scraggy surface.
- UV–Vis spectra were analyzed to study the photophysical properties of Fe ions.
- The Ti–Fe 10 wt. % of iron was more active for hydrogen production.

ARTICLE INFO

Article history:
Received 20 December 2021
Received in revised form
30 March 2022
Accepted 19 April 2022
Available online xxx

Keywords:
Hydrogen production
Ti–Fe mixed Oxides
Photocatalysts
Water splitting

ABSTRACT

Ti–Fe mixed oxides were prepared by sol-gel and used as photocatalysts for the generation H_2 from water. The solids were characterized by SEM-EDS, N_2 physisorption, XRD, UV–Vis and XPS spectroscopy. The mixed oxides present larger specific surface areas (83–205 m^2/g) than that of pure TiO_2 (64 m^2/g). The XRD patterns of the Ti–Fe solids resemble that of anatase titania. The band gap energies of the solids vary from 3.0 to 2.5 eV and are smaller than that of TiO_2 (3.2 eV). The mixed oxides were tested as photocatalysts in the production of hydrogen from water using methanol as a sacrificial agent. In all cases, their catalytic activities were higher than that exhibited by TiO_2 after 10 h of reaction.

* *Corresponding author*. Laboratorio de Investigación en Materiales, agua y energía, Engineering Department, Campus Los Altos, University of Guadalajara, Av. Rafael Casillas Aceves 1200, Tepatitlan de Morelos, Jalisco, 47600, Mexico.
E-mail address: alarios@cualtos.udg.mx (A. Pérez-Larios).

https://doi.org/10.1016/j.ijhydene.2022.04.179
0360-3199/

Introduction

Due to the decrease in the world oil reserves, it is urgent to find a renewable source and reduce the pollution of the environment [1,2] caused by the irresponsible use of fossil fuels. Production of hydrogen from other sources different than fossil fuels is a very attractive to solve the energetic and environmental problems [3,4]. Fujishima and Honda reported that titania can be used as a photocatalyst for the generation of hydrogen from water under UV irradiation [4,5]. Nowadays, the photocatalytic production of hydrogen is considered one of the most promising alternatives to truckle the environmental and energetic problems [6–8]. It is known that for a photocatalytic reaction to occur some stages are necessary: the excitation of a catalyst by an irradiation of wavelength equal or greater than the band gap energy (Eg); as a consequence an electron is transferred from the valence band (VB) to the conduction band (CB) generating a hole and redox reactions occur at the catalyst surface [6]. Titania is one of the most used photocatalyst for the degradation of pollutants and for the production of hydrogen from water [8–12]. Pure titania presents a band gap energy of 3.2 eV and a short photoactivated charge [13]. Various procedures for the synthesis of Ti–Fe mixed oxides are reported in the literature, for instance, electrochemical deposition, vapour autodeposition, atomic layer deposition, mechanochemical, hydrothermal and sol-gel synthesis [12–20]. The sol–gel technique is considered one of the many approaches used for the synthesis and fabrication of metal oxides nanoparticles as well as metal oxides nanocomposites [1]. The sol–gel method has many features that distinguish it from other techniques [21–24]. The main peculiarity that makes the sol– gel route unique is the formation of colloidal suspension that is caused by the condensation of dissolved precursors. The second merit is the integration and combining of the colloidal particles during the gelation phase into a polymetric matrix by means of chemical reactions that bond the local reactive groups at their surface and the materials obtained from the sol–gel route can be used in heterogeneous photocatalysis processes [23–27]. The presence of iron into the structure of the titania enhances the photochemical stability. Doping of Fe^{3+} ion in the matrix of titania is most favored owing to the similar size of Ti^{4+} ions, and its low bandgap energy [28,29]. In addition, iron is very attractive (α-Fe_2O_3) because is one of the most abundant elements on earth, is affordable, no toxic and is an n-type semiconductor that possesses a band-gap in the range of 2.0–2.2 eV, is considered a suitable semiconductor for hydrogen (H_2) production and it is capable of absorbing light photons in the visible spectrum ~600 nm Fe^{3+} cations can act as a sinker of photogenerated e^-/h^+ pairs in the titania lattice, leading to improve charge separation and as a result, enhanced the photoactivity [8,30]. It was previously reported that Ti–Fe nanomaterials are efficient photocatalysts [31]. Furthermore, the morphology of these materials plays an important role in photocatalysts. In this respect, Shenimin Zhu et al. [30] found that mesoporosity is very important. In the present study, the effect of the addition of iron into the titania structure on the photocatalytic production of hydrogen is explored. Additionally, the catalysts were also characterized by SEM-EDS, XRD, N_2 physisorption, UV–Vis and XPS spectroscopies.

Experimental

Catalyst preparation

Ti–Fe mixed oxides were prepared by the sol-gel using titanium (IV) butoxide (Aldrich 97%) and iron nitrate (Reasol 99%) as precursors. To this aim, 130 mL of ethanol (Aldrich 98%) containing the required amount of $Fe(NO_3)_3 \cdot 9H_2O$ to obtain solids with 1.0, 3.0, 5.0 and 10.0 wt. % of Fe. The solution was then heated up under a reflux to 70 °C and a dwell of 2 h was applied. After cooling down to ambient temperature, the solution was then kept at 0 °C for 6 h. The mixture was then under sonication during 30 min and afterwards kept at 4 °C for 12 h. Calcination in static air was then performed, heating up the sample from ambient temperature to 500 °C using a heating rate of 1 °C/min. Once at the final temperature a dwell of 5 h was applied. Similarly, pure titania was also synthesized and used as a reference. The solid were then ground in a mortar [31]. For identification the samples were labeled as Ti–Fe-X where X is the percentage of iron in the solid.

Characterization

Morphology

The surface morphology of the mixed oxide powder was determined using a scanning electron microscopy (SEM) (Tescan, MIRA 3LMU) at 20 kV, equipped with an Energy Dispersive Spectroscopy (Bruker, QUANTAX) accessory, which was utilized to determine the elemental analysis of the mixed oxide samples [30].

Physisorption of N_2

Nitrogen adsorption-desorption isotherms were evaluated and then used to determine the textural properties of the samples, using a Micromeritics instrument, TriStar II Plus. The samples were first degassed at 200 °C for 3 h at low pressure, and the adsorption-desorption isotherms were then acquired at liquid N_2 temperature (77 K), and in the pressures range from 10^{-6} to 1.0 P/P_0. The specific surface areas were calculated by using the Brunauer-Emmett-Teller (BET) procedure and the pore size distribution was obtained according to the Barret-Joyner-Halenda (BJH) method [31].

X-ray diffraction

The diffraction patterns for the Ti–Fe mixed oxides were acquired on a X-ray diffractometer (Panalytical Empyrean) equipped with Cu Kα radiation (λ = 0.154 nm). The diffraction intensities as a function of the 2Θ angle were measured between 10 and 90°, using a step size of 0.02° and a counting time of 0.2 s per step [32]. Furthermore, the average crystal size was determined by the Scherer's equation and using the most intense diffraction for each sample as a reference:

$$D = \frac{K\lambda}{\beta \mathrm{Cos}(\theta)} \quad (1)$$

where K is shape factor (0.89), λ is the X ray wavelength (0.154 nm), β is the peak broadening at half maximum and Θ is the Bragg angle.

Please cite this article as: Pérez-Larios A et al., Ti–Fe mixed oxides as photocatalysts in the generation of hydrogen under UV-light irradiation, International Journal of Hydrogen Energy, https://doi.org/10.1016/j.ijhydene.2022.04.179

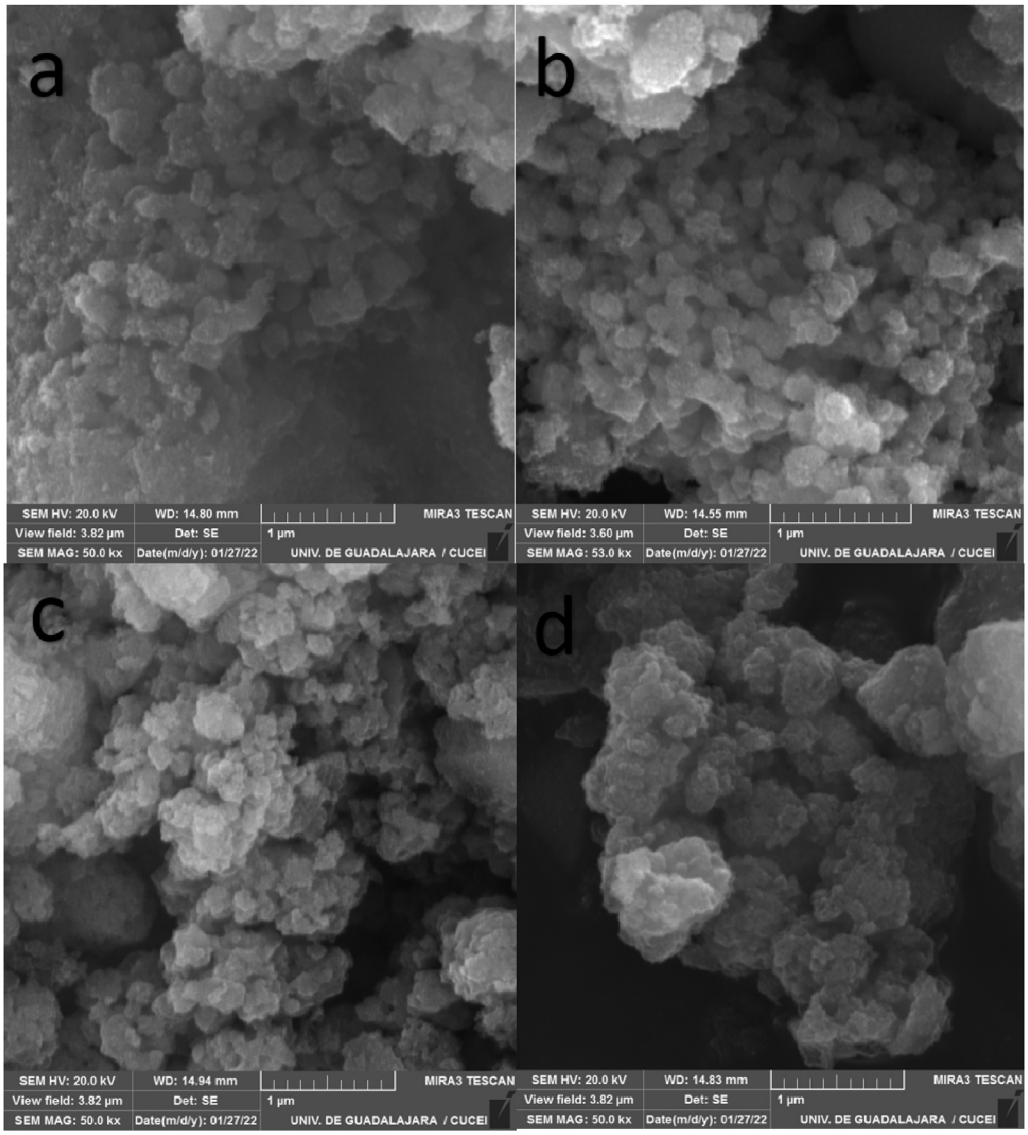

Fig. 1 – The SEM-images of the samples (a: Ti–Fe1, b: Ti–Fe3, c: Ti–Fe5 and d: Ti–Fe10).

Table 1 – Elemental composition determined by EDS.

Element	Weight (%)			
	Ti–Fe1	Ti–Fe3	Ti–Fe5	Ti–Fe10
Ti	27	39	50	61
Fe	1.5	3.4	4.7	9
O	71.5	57.6	45.3	30

Additionally, the interplanar spacing (d) can be calculated from the Bragg's law equation:

$$d(\text{Å}) = \frac{n\lambda}{2\sin\theta} \quad (2)$$

UV–vis diffuse reflectance spectroscopy

The UV–Vis absorption spectra were obtained using a UV–Vis spectrophotometer (Shimadzu UV-2600, Japan). The

Table 2 – Textural properties, band gap energy (Eg) and H_2 production for the Ti–Fe samples.

Fe (wt. %)	SSA (m^2/g)	Mean pore diameter (nm)	Cell parameter *a* (Å)	Crystallite size (nm) D	Eg (eV)	H_2 production (µmol/h)
1	83	7.1	4.85	6.1	3.0	1548
3	108	7.6	4.36	6.3	2.8	1703
5	121	7.8	3.75	6.4	2.7	4193
10	205	7.9	3.53	7.0	2.5	5586
TiO_2	64	6.5	3.77	5.7	3.2	190

Please cite this article as: Pérez-Larios A et al., Ti–Fe mixed oxides as photocatalysts in the generation of hydrogen under UV-light irradiation, International Journal of Hydrogen Energy, https://doi.org/10.1016/j.ijhydene.2022.04.179

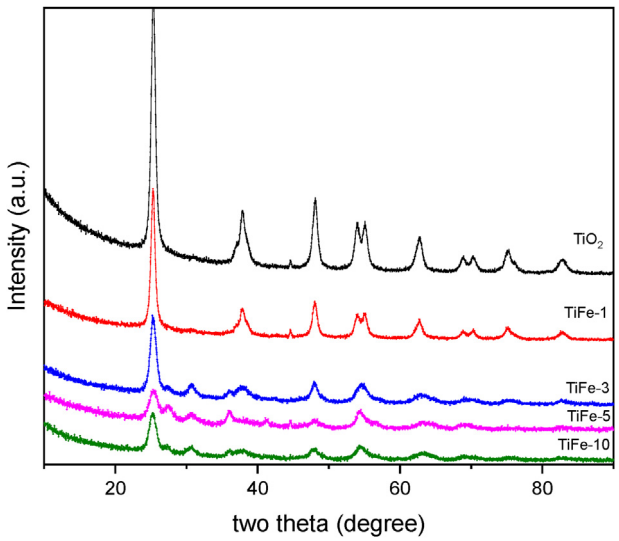

Fig. 2 – X-ray diffraction patterns of the Ti–Fe samples.

instrument is coupled with an integration sphere for diffuse reflectance studies. The equipment was calibrated with barium sulfate and it was used as a reference [28]. The optical absorption was measured in the wavelength range from 190 to 900 nm. From the spectra, the band gap energy was calculated using the following empirical equation:

$$Eg = \frac{hc}{\lambda} \quad (3)$$

where Eg is the band gap energy; h is the Plank's constant equal to 6.626×10^{-34} J*s; c is the velocity of light equal to 2.99×10^{8} m/s and λ is the wavelength.

XPS spectroscopy

X-ray photoelectron spectroscopic (XPS) analyses was performed using a SPEC Phoibos 150 equipment operated at 10 mbar and provided with a monochromatized Al Ka X-ray source (1487 eV). The position of the O1s peak at 530.0 eV was monitored on each sample to ensure that no binding energy shift due to charging had occurred. Narrow scans were collected at 60 eV analyzer pass energy and at 400 mm spot size. The samples were deposited over a film of In in order to minimize the charge effects [33].

Photocatalytic test

A closed reaction system previously reported elsewhere [31], was used for this purpose. A homemade Pyrex reactor of 250 mL was initially filled with 200 mL of a water-methanol solution (1:1 vol) and 0.1 g of catalyst. Methanol was used as a sacrificial compound. The reaction system was initially filled with N_2. A gas chromatograph was also connected within the reaction system. During reaction, nitrogen and

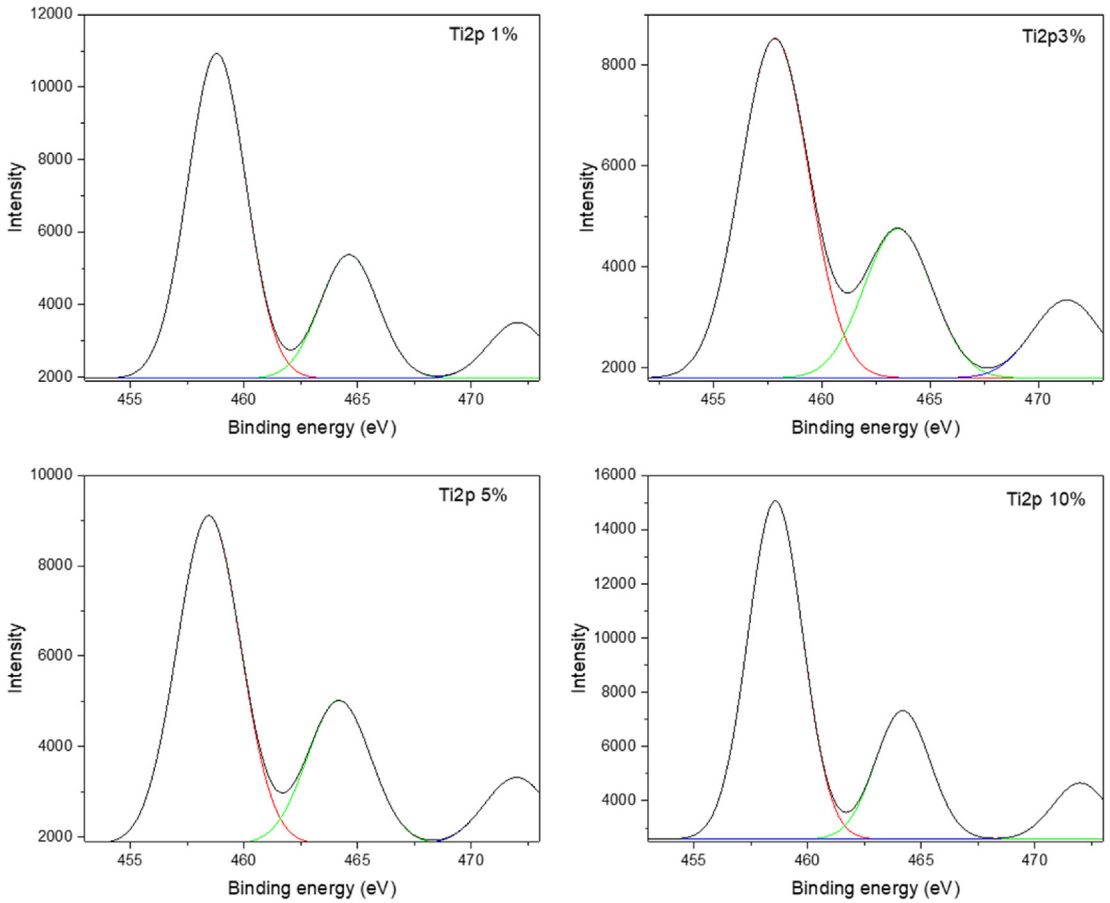

Fig. 3 – Ti 2p XPS spectra of the Ti–Fe samples.

Please cite this article as: Pérez-Larios A et al., Ti–Fe mixed oxides as photocatalysts in the generation of hydrogen under UV-light irradiation, International Journal of Hydrogen Energy, https://doi.org/10.1016/j.ijhydene.2022.04.179

hydrogen produced during the photocatalytic test continuously circulate the system using a peristaltic pump. For hydrogen quantification, gas samples were analyzed periodically with a Varian CP-3800 gas chromatograph equipped with a thermal conductivity detector and a 5 A molecular sieve column (30 m length, 0.35 mm ID and 50 mm OD). The system was also provided with a water trap to protect the GC-column and with a high-pressure UV Hg pen–lamp (254 nm and 2.2 mW/cm^2) which was placed into a quartz tube and immersed in the water–methanol solution during the photocatalytic reaction.

Result and discussion

EDS spectroscopy analysis

The SEM images of mixed oxides are shown in Fig. 1 (a,b,c,d). The images reveal agglomeration of rounded and irregular shape particles. Agglomeration is commonly observed in solids synthetized by sol-gel [31–34]. The surface elemental composition of the mixed oxides is presented in Table 1, and was determined by the EDS attached to the SEM. The weight percentages are closed to the nominal composition.

N_2 physisorption

The specific surface areas (SSA) of the samples after calcination at 500 °C are reported in Table 2. All SSA are larger than that of pure TiO_2. Both the SSA and mean pore diameter increase as the content of iron augments. Pure TiO_2 showed a SSA of 64 m^2/g, pore diameter of 6.5 nm. However, the SSA (83–205 m^2/g), pore diameter (7.1–7.9 nm) of the nanocomposites varied depending on the Fe wt. % [30].

X-ray diffraction

The crystalline structure of the Ti–Fe mixed oxides was determined by XRD. The diffractograms of the samples resemble that of anatase titania and are presented in Fig. 2. Anatase titania presents diffractions at 25.3, 37.9, 47.8, 54.5, 55, 62.5, 69, 70, 75 and 82° 2Θ which accordingly to JCPDS 21–1272, correspond to (101), (103), (200), (105), (211), (204), (116), (220), (215) and (303) planes, respectively. Diffractions at about 27.5 and 30.6, 36.1° merge as the iron content increases above 3 wt. %. In addition, the intensities of all diffractions decrease and the broadness augments compared to the respective peaks of the anatase titania. Assignation of the diffractions at 27.5 and 30.6, 36.1° is still unclear. If some Fe_2TiO_5 would have formed, the XRD diffractions would be at 18.16, 25.72, 32.72, 37.5, 55.37 and 59.99° [29,30]. However, the maximum Fe/Ti atomic ratio used in our experiments was 0.095 which is far from 2 accordingly to the stoichiometry of Fe_2TiO_5. Segregation of iron species above 1 wt. % was therefore assumed. Such iron species would be well distributed and out of the detection limit of the instrument. Since a shift of the main titania diffraction at about 25.3°, assigned to (101) plane, was unnoticed in Ti–Fe1 sample, it demonstrates again that iron is well distributed in the titanium

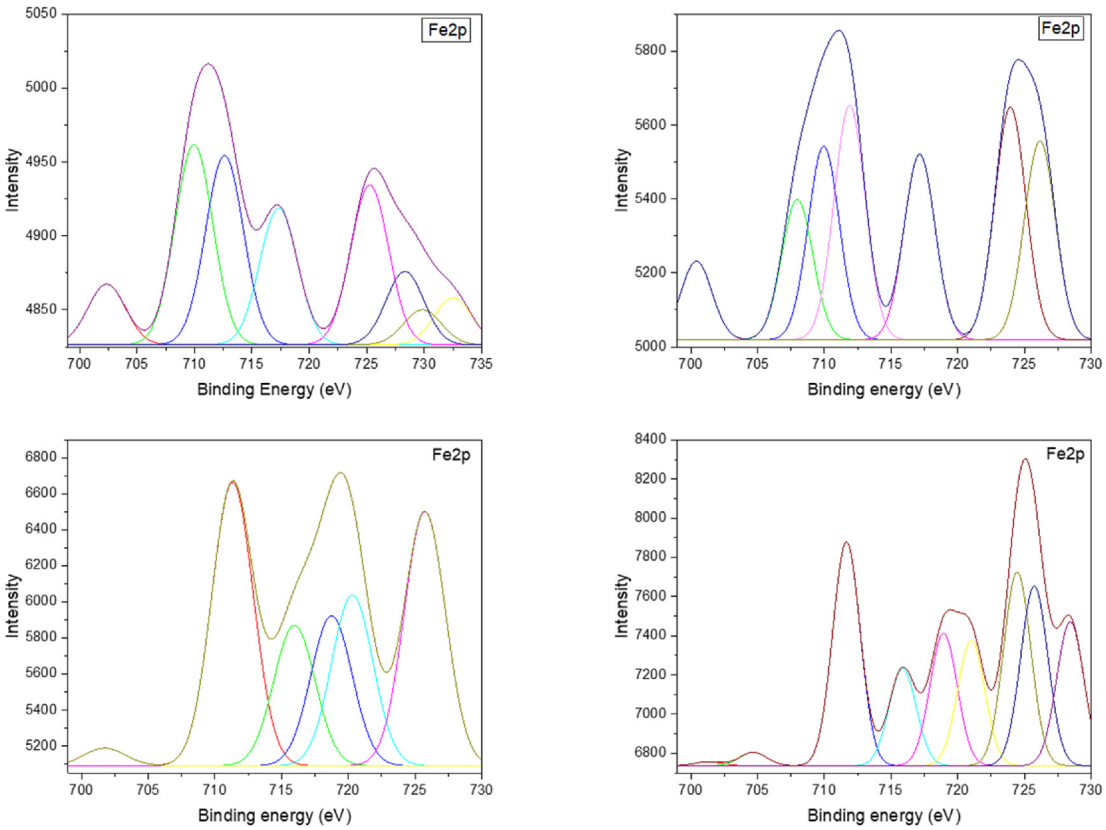

Fig. 4 – Fe 2p XPS spectra of the Ti–Fe samples.

Please cite this article as: Pérez-Larios A et al., Ti–Fe mixed oxides as photocatalysts in the generation of hydrogen under UV-light irradiation, International Journal of Hydrogen Energy, https://doi.org/10.1016/j.ijhydene.2022.04.179

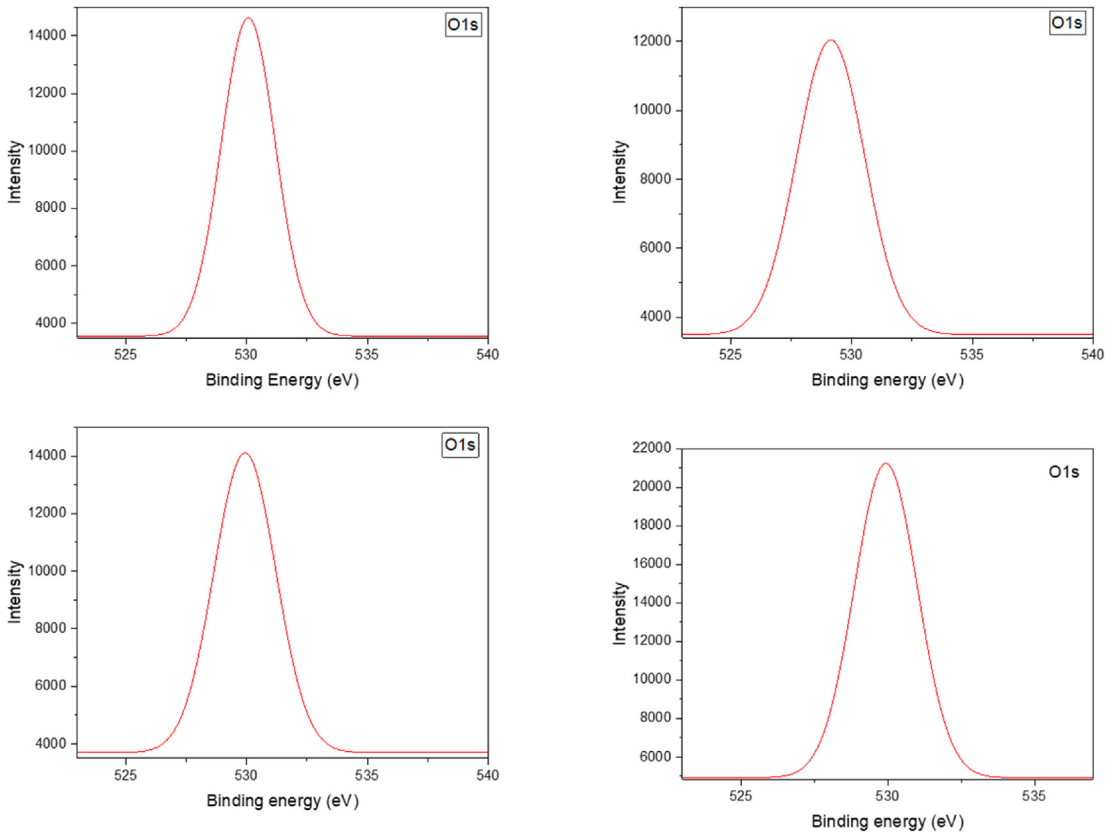

Fig. 5 – O 1s XPS spectra of the Ti–Fe samples.

oxide structure. The crystallite size (D) and cell parameter (*a*) were estimated from the peak at 25.3° and reported in Table 2. The *a* values range from 3.53 to 4.85 nm whereas D varies from 6.1 to 7.0 Å and are greater than that of pure titania (5.7 nm).

UV–vis diffuse reflectance spectroscopy

UV–Vis spectra were recorded to analyze the effect of iron on the photophysical properties of Ti–Fe photocatalysts. Table 2, shows the UV–Vis DRS spectra of the materials. All samples exhibit an optical absorption below 400 nm, which can be attributed to electron Ti–O transition of titania nanocrystalline. The results show a small shift to the red region (3.0–2.5 eV) for the Ti–Fe samples in comparison to pure TiO_2 (3.2 eV) [30]. The incorporation of Fe into titanium oxide presents some variations in the band gap energy, Eg Ref. [32]. Some authors have reported that Eg may be influenced by other factors such as morphology, size and doping material concentration [36]. It was previously reported that the position of the valence band edge of TiO_2 remains unaltered after metal ions are incorporated into this oxide; however, addition of Fe ions introduce new energy levels into the band gap of TiO_2. As a result, the shift in the absorption edges toward longer wavelengths for the Fe-doped TiO_2 should come from the electronic transition from the Fe^{3+}/Fe^{4+} energy level to the conduction band of TiO_2. Reduction in the band gap energies of the Fe-doped TiO_2 samples were also noted previously [37,38].

XPS spectroscopy

To determine the chemical states of the species on the surface of the Ti–Fe mixed oxides, the XPS spectra were acquired and analyzed. The deconvolution of the spectra are also presented within the figures. Figs. 3–5 show the Ti 2p, Fe 2p and O 1s spectra of the TiO_2 and Ti–Fe catalysts, respectively. The binding energies of anatase titania are located at 459.09,

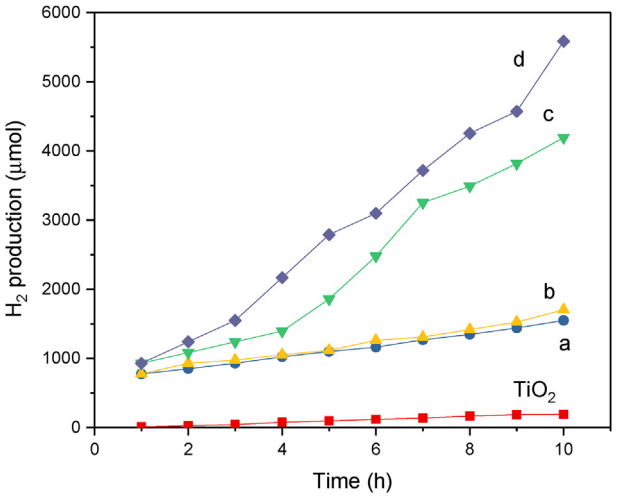

Fig. 6 – H_2 production profiles using Ti and the Ti–Fe as photocatalysts, (a: TiFe-1, b: TiFe-3, c: TiFe-5 and d: TiFe-10).

Please cite this article as: Pérez-Larios A et al., Ti–Fe mixed oxides as photocatalysts in the generation of hydrogen under UV-light irradiation, International Journal of Hydrogen Energy, https://doi.org/10.1016/j.ijhydene.2022.04.179

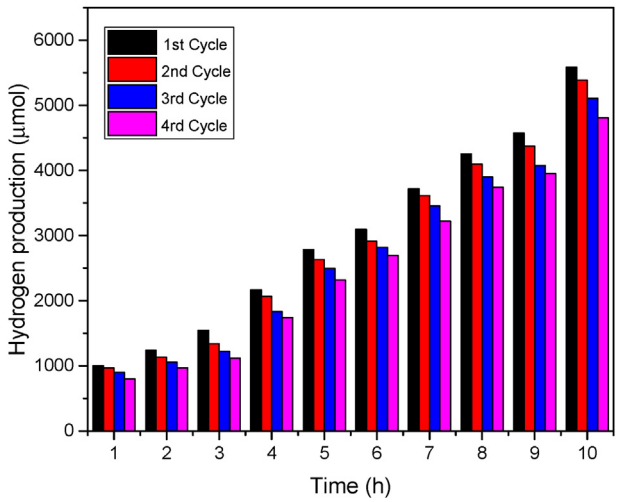

Fig. 7 – Hydrogen production profile of the Ti–Fe10 catalyst after four cycles.

464.74 and 472.41 eV and are assigned to Ti $2p_{3/2}$, Ti $2p_{1/2}$ and Ti–OH, accordingly. The main Ti $2p_{3/2}$ signal at about 459 eV slightly changes to 458.77, 457.83, 458.44 and 458.59 eV for the Ti–Fe samples containing 1, 3, 5, and 10 wt. % of Fe. Accordingly to the XRD pattern of the TiFe-1 sample, Fe is well distributed in the titanium structure, possible located in the interstitial spaces and/or replacing some Ti atoms, since such a replacement was reported to occur at low Fe content [39]. Above 1 wt. % of iron in the Ti–Fe samples, segregation of iron is likely to occur. Such iron species could be amorphous and remain therefore undetectable by XRD. In addition, the expected Fe 2p XPS spectra would be complex.

Indeed, Fig. 5 shows such Fe 2p spectra, which agree well with the formation of various iron oxides. Once segregated, iron could be present as Fe^{2+} and Fe^{3+} species. Fe^0 is unexpected since the synthesis was conducted under non-reducible conditions. At least, iron species such as FeO, Fe_2O_3 and Fe_3O_4 are therefore expected. Binding energies for Fe $2p_{3/2}$ and Fe $2p_{1/2}$ of FeO are located at 709.53, 723.17, respectively and a satellite at 715.62 eV. For Fe_2O_3, the Fe $2p_{3/2}$ and Fe $2p_{1/2}$ peaks are observed at 711, 724.6 eV and a satellite at 718.8 eV, whereas those for Fe_3O_4 are located at about 710.6 and 724.1 eV, respectively [33]. In addition, multiplets were found to fit well the complex XPS Fe2p spectra of Fe_3O_4 where both Fe^{2+} and Fe^{3+} are present [40]. Fe_3O_4 could be represented as a mixture of two iron phases: FeO and F_2O_3 which implies therefore that Fe^{2+}: Fe^{3+} would theoretically be 1:2. Consequently, the complex Fe 2p XPS spectra reported in Fig. 4 indicates the presence of iron oxide mixtures containing at least the three phases described above. Other compounds such as α-Fe_2O_3, γ-Fe_2/O_3, γ-FeOOH and γ-FeOOH might also be present in our samples.

The O 1s spectrum for pure titania shows a strong signal at about 530 eV which marginally turns to lower energies as the Fe content augments, Fig. 5.

Photocatalytic evaluation

Fig. 6 shows the hydrogen production as a function of the irradiation time for pure anatase titania and Ti–Fe photocatalysts. It can be seen that the hydrogen generation

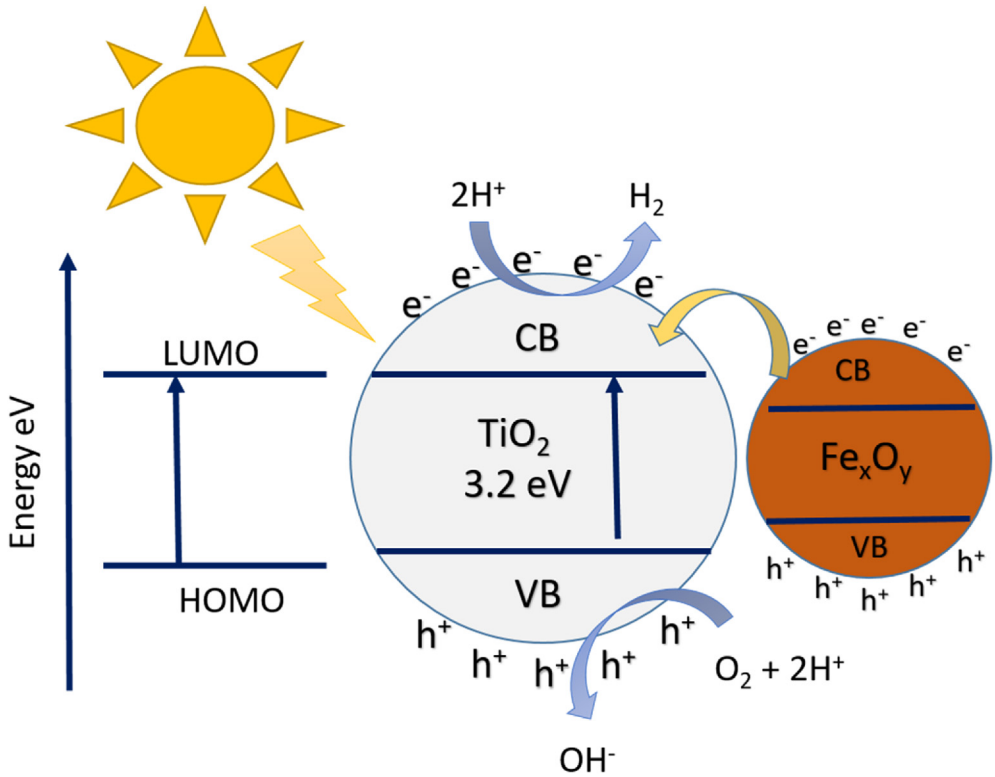

Fig. 8 – A schematic diagram of the proposed hydrogen generation mechanism on Fe–Ti photocatalysts.

Please cite this article as: Pérez-Larios A et al., Ti–Fe mixed oxides as photocatalysts in the generation of hydrogen under UV-light irradiation, International Journal of Hydrogen Energy, https://doi.org/10.1016/j.ijhydene.2022.04.179

increases as the Fe content augments. Mean hydrogen production rates were calculated assuming straight line fittings during the catalytic experiments. Consequently, a hydrogen generation rate for pure TiO_2 was 190 μmol/h, while greater values such as 1548, 1703, 4193 and 5586 μmol/h were determined for Ti–Fe1, Ti–Fe3, Ti–Fe5, and Ti–Fe10, respectively. These mixed oxide were therefore more active than that observed for pure anatase titania [37–41]. Fig. 7, presents the performance of the Ti–Fe10 sample as a promising catalyst in the generation of hydrogen after four cycles and under UV light irradiation.

Photocatalytic hydrogen mechanism

The following hydrogen mechanism is similar to that previously proposed using Fe-doped titania photocatalysts [8]. Briefly, upon suitable irradiation of the photocatalytic surface, electrons (e^-) and holes (h^+) are generated and transferred to the surface to perform reduction and oxidation reactions. The presence of various Fe species on the modified titania surface resulted in a reduction of the band gap relative to pure titania, and in an enhancement of the charge transfer by retarding the recombination of the electron/holes pairs, as indirectly observed in the photocatalytic hydrogen experiments. The stable Fe^{3+} species capture electrons to form Fe^{2+} and holes to produce Fe^{4+} species [42]. Afterwards and due to the instability of Fe^{2+} and Fe^{4+} compared to Fe^{3+} [43], the trapped charges will be released and migrate to the surface [44]. Once at the surface, the electrons would react with H^+ to produce H_2 whereas h^+ would strongly oxidise methanol, used as sacrificial reagent, to finally produce CO_2 and H_2O. Fig. 8 shows a schematic diagram of the proposed hydrogen evolution mechanism.

Conclusion

Ti–Fe mixed oxides with 1–10 wt. % of iron were prepared by sol–gel and tested as photocatalysts in the generation of hydrogen from water using methanol as a sacrificial agent, and under UV irradiation. All Ti–Fe samples showed greater catalytic activity than that observed for pure anatase titania. Characterization indicates that above 1 wt. % of Fe in the Ti–Fe samples, segregation is likely to occur leading to solids with greater photocatalytic activities for the hydrogen production than that measured for pure anatase titania. In addition, all Ti–Fe catalysts presented great photocatalytic activites after four runs. Under UV light, the best catalytic activity among our samples, was observed for the Ti–Fe10 mixed oxide with an average hydrogen rate of 5586 μmol/h which was greater than that of pure anatase titania, 190 μmol/h.

Declaration of competing interest

The authors declare that they have no known competing financial interests or personal relationships that could have appeared to influence the work reported in this paper.

Acknowledgments

Pérez-Larios A., thanks to CONACYT, I appreciate the support in the characterization of the photocatalysts from Dr. Martin Flores and Dr. Milton Vázquez as well as technicians of the equipment Ing. Sergio Oliva and Ms. José Rivera for the characterization of XRD, SEM and XPS analysis (Proyect: 270660, Support for the Strengthening and Development of the Scientific and Technological Infrastructure).

REFERENCES

[1] Abbas N, Shao GN, Haider MS, Imran SM, Park SS, Kim HT. Sol–gel synthesis of TiO_2-Fe_2O_3 systems: effects of Fe_2O_3 content and their photocatalytic properties. J Ind Eng Chem 2016;39:112–20.
[2] Banisharif A, Khodadadi AA, Mortazavi Y, Anaraki Firooz A, Beheshtian J, Agah S, et al. Highly active Fe_2O_3-doped TiO_2 photocatalyst for degradation of trichloroethylene in air under UV and visible light irradiation: experimental and computational studies. Appl Catal B Environ 2015;165:209–21.
[3] Bashiri R, Irfan MS, Mohamed NM, Sufian S, Ling LY, Suhaimi NA, et al. Hierarchically SrTiO3@TiO_2@Fe_2O_3 nanorod heterostructures for enhanced photoelectrochemical water splitting. Int J Hydrogen Energy 2020;46(48):24607–19. https://doi.org/10.1016/j.ijhydene.2020.02.106.
[4] Bashiri R, Samsudin MFR, Mohamed NM, Suhaimi NA, Ling LY, Sufian S, et al. Influence of growth time on photoelectrical characteristics and photocatalytic hydrogen production of decorated Fe_2O_3 on TiO_2 nanorod in photoelectrochemical cell. Appl Surf Sci 2020:510.
[5] Bashiri R, Samsudin MFR, Mohamed NM, Suhaimi NA, Ling LY, Sufian S, et al. Influence of growth time on photoelectrical characteristics and photocatalytic hydrogen production of decorated Fe_2O_3 on TiO_2 nanorod in photoelectrochemical cell. Appl Surf Sci 2020:510.
[6] Ismael Mohomed. The photocatalytic performance of the ZnO/g-C_3N_4 composite photocatalyst toward degradation of organic pollutants and its inactivity toward hydrogen evolution: the influence of light irradiation and charge transfer. Chem Phys Lett 2020;739:136992.
[7] Mohammed I, Wu Y, Warl M. Photocatalytic activity of ZrO_2 composites with graphitic carbón nitride for hydrogen production under visible light. New J Chem 2019;43:4455–62.
[8] Mohammed I. Enhanced photocatalytic hydrogen production and degradation of organic pollutants from Fe(III) doped TiO_2 nanoparticles. J Environ Chem Eng 2020;8:103676.
[9] Mohammed I. Highly effective ruthenium-doped TiO_2 nanoparticles photocatalyst for visible-light-driven photocatalytic hydrogen production. New J Chem 2019;43:9596.
[10] Li Y, Yang B, Liu B. MOF assisted synthesis of TiO_2/Au/Fe_2O_3 hybrids with enhanced photocatalytic hydrogen production and simultaneous removal of toxic phenolic compounds. J Mol Liq 2021;322:114815.
[11] Madhumitha A, Preethi V, Kanmani S. Photocatalytic hydrogen production using TiO_2 coated iron-oxide core shell particles. Int J Hydrogen Energy 2018;43:3946–56.
[12] Mohamed RM, Kadi MW, Ismail AA. A Facile synthesis of mesoporous α-Fe_2O_3/TiO_2 nanocomposites for hydrogen evolution under visible light. Ceram Int 2020;46:15604–12.

Please cite this article as: Pérez-Larios A et al., Ti–Fe mixed oxides as photocatalysts in the generation of hydrogen under UV-light irradiation, International Journal of Hydrogen Energy, https://doi.org/10.1016/j.ijhydene.2022.04.179

[13] Palanisamy B, Babu CM, Sundaravel B, Anandan S, Murugesan V. Sol-gel synthesis of mesoporous mixed Fe_2O_3/TiO_2 photocatalyst: application for degradation of 4-chlorophenol. J Hazard Mater 2013;252–253:233–42.
[14] Pang YL, Lim S, Ong HC, Chong WT. Synthesis, characteristics and sonocatalytic activities of calcined γ-Fe_2O_3 and TiO_2 nanotubes/γ-Fe_2O_3 magnetic catalysts in the degradation of Orange G. Ultrason Sonochem 2016;29:317–27.
[15] Preethi V, Kanmani S. Photocatalytic hydrogen production using Fe_2O_3-based core shell nano particles with ZnS and CdS. Int J Hydrogen Energy 2014;39:1613–22.
[16] Sánchez Mora E, Gómez Barojas E, Rojas Rojas E, Silva González R. Morphological, optical and photocatalytic properties of TiO_2-Fe_2O_3 multilayers. Sol Energy Mater Sol Cells 2007;91:1412–5.
[17] Sołtys-Mróz M, Syrek K, Pierzchała J, Wiercigroch E, Malek K, Sulka GD. Band gap engineering of nanotubular Fe_2O_3-TiO_2 photoanodes by wet impregnation. Appl Surf Sci 2020:517.
[18] Wang T, Yang G, Liu J, Yang B, Ding S, Yan Z, et al. Orthogonal synthesis, structural characteristics, and enhanced visible-light photocatalysis of mesoporous Fe_2O_3/TiO_2 heterostructured microspheres. Appl Surf Sci 2014;311:314–23.
[19] Wu L, Yan H, Xiao J, Li X, Wang X, Zhao T. Characterization and photocatalytic properties of nano-Fe_2O_3–TiO_2 composites prepared through the gaseous detonation method. Ceram Int 2017;43:14334–9.
[20] Su C, Hong B-Y, Tseng C-M. Sol–gel preparation and photocatalysis of titanium dioxide. Catal Today 2004;96:119–26.
[21] Akpan UG, Hameed BH. The advancements in sol–gel method of doped-TiO_2 photocatalysts. Appl Catal Gen 2010;375:1–11.
[22] Moradi H, Eshaghi A, Hosseini SR, Ghani K. Fabrication of Fe-doped TiO_2 nanoparticles and investigation of photocatalytic decolorization of reactive red 198 under visible light irradiation. Ultrason Sonochem 2016;32:314–9.
[23] Yang Y, Wang P. Preparation and characterizations of a new PS/TiO_2 hybrid membranes by sol–gel process. Polymer 2006;47:2683–8.
[24] Landau MV. Sol-gel processing. In: de Jong KP, editor. Synthesis of solid catalysts. John Wiley & Sons; 2009. p. 83–109.
[25] Cao X, Luo S, Liu C, Chen J. Synthesis of bentonite-supported Fe_2O_3-doped TiO_2 superstructures for highly promoted photocatalytic activity and recyclability. Adv Powder Technol 2017;28:993–9.
[26] Nasralla N, Yeganeh M, Astuti Y, Pitticharoenphun S, Shahtahmasebi N, Kompany A, Karimipour M, Mendis BG, Poolton NRJ, Šiller L. Structural and spectroscopic study of Fe-doped TiO_2 nanoparticles prepared by sol–gel method. Sci Iran 2013;20:1018–22.
[27] Khaki MRD, Shafeeyan MS, Raman AAA, Daud WMAW. Application of doped photocatalysts for organic pollutant degradation - a review. J Environ Manag 2017;198:78–94.
[28] Yao H, Liu L, Fu W, Yang H, Shi Y. Fe_2O_3 nanothorns sensitized two-dimensional TiO_2 nanosheets for highly efficient solar energy conversion. FlatChem 2017;3:1–7.
[29] Yao K, Basnet P, Sessions H, Larsen GK, Murph SEH, Zhao Y. Fe_2O_3-TiO_2 core-shell nanorod arrays for visible light photocatalytic applications. Catal Today 2016;270:51–8.
[30] Zhu S, Yao F, Yin C, Li Y, Peng W, Ma J, et al. Fe_2O_3/TiO_2 photocatalyst of hierarchical structure for H_2 production from water under visible light irradiation. Microporous Mesoporous Mater 2014;190:10–6.
[31] Pérez-Larios A, Lopez R, Hernández-Gordillo A, Tzompantzi F, Gómez R, Torres-Guerra LM. Improved hydrogen production from water splitting using TiO_2-ZnO mixed oxides photocatalysts. Fuel 2012;100:139–43.
[32] Pérez-Larios A, Hernández-Gordillo A, Morales-Mendoza G, Lartundo-Rojas L, Mantilla Á, Gómez R. Enhancing the H2 evolution from water-methanol solution using Mn^{2+}-Mn^{+3}-Mn^{4+} redox species of Mn-doped TiO_2 sol-gel photocatalysts. Catal Today 2016;266:9–16.
[33] Anaya-Esparza LM, Montalvo-González E, González-Silva N, Méndez-Robles MD, Romero-Toledo R, Yahia EM, et al. Synthesis and characterization of TiO_2-ZnO-MgO mixed oxide and their antibacterial activity. Materials 2019;12.
[34] Pérez-Larios A, Rico JL, Anaya-Esparza LM, Vargas OAG, González-Silva N, Gómez R. Hydrogen production from aqueous methanol solutions using Ti–Zr mixed oxides as photocatalysts under UV irradiation. Catalysts 2019;9.
[36] Avilés-García O, Espino-Valencia J, Romero-Romero R, Rico-Cerda JL, Arroyo-Albiter M, Solís-Casados DA, et al. Enhanced photocatalytic activity of titania by co-doping with Mo and W. Catalysts 2018;8. https://doi.org/10.3390/catal8120631.
[37] Ngo HD, Ngo TD, Tamanai A, Chen K, Cuong NT, U N, Handegard OS, Pucci A, Umezawa N, Nabatame T, Nagao T. Structure and optical properties of sputter deposited pseudobrookite Fe_2TiO_5 thin films. CrystEngComm 2019;21:34–40.
[38] Wu T, Zhu X, Xing Z, Mou S, Li C, Qiao Y, Liu Q, Zhang Y, Sun X. Greatly improving electrochemical N 2 reduction over TiO_2 nanoparticles by iron doping. Angew Chem Int Ed 2019;58:18449–53.
[39] Yamashita T, Hayes P. Analysis of XPS spectra of Fe^{2+} and Fe^{3+} ions in oxide materials. Appl Surf Sci 2008;254:2441–9.
[40] Grosvenor AP, Kobe BA, Biesinger MC, McIntyre NS. Investigation of multiplet splitting of Fe 2p XPS spectra and bonding in iron compounds. Surf Interface Anal 2004;36:1564–74.
[41] Bapna K, Phase DM, Choudhary RJ. Study of valence band structure of Fe doped anatase TiO2 thin films. J Appl Phys 2011;110:2–8.
[42] Choi W, Termin A, Hoffmann MR. The role of metal ion dopants in quantum-sized TiO_2: correlation between photoreactivity and charge carrier recombination dynamics. J Phys Chem 1994;98:13669–79.
[43] Nagaveni K, Hegde MS, Madras G. Structure and photocatalytic activity of $Ti_{1-x}M_xO_{2\pm\delta}$ (M=W, V, Ce, Zr, Fe, and Cu) synthesized by solution combustion method. J Phys Chem B 2004;108:20204–12.
[44] Tong T, Zhang J, Tian B, Chen F, He D. Preparation of Fe^{+}-doped TiO_2 Catalysts by controlled hydrolysis of titanium alkoxide and study on their photocatalytic activity for methyl orange degradation. J Hazard Mater 2008;155:572–9.

Please cite this article as: Pérez-Larios A et al., Ti–Fe mixed oxides as photocatalysts in the generation of hydrogen under UV-light irradiation, International Journal of Hydrogen Energy, https://doi.org/10.1016/j.ijhydene.2022.04.179